# Protonic ceramic electrochemical cells in a metal supported architecture: challenges, status and prospects

To cite this article: Noriko Sata and Rémi Costa 2024 *Prog. Energy* **6** 032002

IOP Publishing Prog. Energy 6 (2024) 032002 https://doi.org/10.1088/2516-1083/ad3f6b

Progress in Energy



OPEN ACCESS

RECEIVED
2 February 2024

REVISED
29 March 2024

ACCEPTED FOR PUBLICATION
16 April 2024

PUBLISHED
7 May 2024





TOPICAL REVIEW

# Protonic ceramic electrochemical cells in a metal supported architecture: challenges, status and prospects

**Noriko Sata*** and **Rémi Costa**

DLR, Institute of Engineering Thermodynamics, Electrochemical Energy Technology, Pfaffenwaldring 38-40, Stuttgart D-70569, Germany

* Author to whom any correspondence should be addressed.

**E-mail:** noriko.sata@dlr.de

**Keywords:** metal supported cells, protonic ceramic cells, fuel cell, electrolysis cell, electrochemical energy conversion device

## Abstract

Protonic ceramic cells (PCCs) offer variety of potential applications for electrochemical energy conversion, however a lot of challenges remain in the development of PCCs for industrial scale manufacturing processes. As it was successfully demonstrated for the solid oxide cells, metal supported architecture is a good alternative for PCCs with many attractive advantages in terms of stabilities in operation and reduction of raw critical materials. In this review, proposed architectures, component materials and processing options are summarized. The challenges and prospects are discussed.

## 1. Introduction

Electrochemical energy conversion based on proton conducting ceramic cells, or protonic ceramic cells (PCCs) is promising in hydrogen production, electrochemical synthesis as well as power generation, i.e. fuel cell operation. Nonetheless, the development of PCC is far behind the other relevant technologies, e.g. proton exchange membranes and solid oxide cells (SOCs). SOC technologies had a significant progress in the last decades and are approaching of maturity for commercialization that promotes the development of high temperature electrochemical devices.

Built upon oxygen ion conducting or proton conducting ceramic materials, mechanical robustness of SOC and PCC, sufficient for handling, stacking and operating at high temperature, is conferred by increasing the thickness of one of the constitutive cell layers that can be either the electrolyte or one out of the two electrodes. This requires a substantial amount of ceramic and critical raw materials and often enforces compromises in terms of performance.

The metal supported cell (MSC) design aims at replacing thick ceramic-based electrode supports by metallic substrates, capable of withstanding both oxidizing and reducing environment at the processing and operational temperatures and capable of supporting thin ceramic layers. MSC architecture provides many advantages for SOCs and PCCs: mechanical stabilities, tolerance to redox cycling, fast start-up capability as well as cost reduction of structural materials. The excellence of MSC architecture has been demonstrated for SOCs.

Different concepts of metal supported SOCs (MS-SOCs) have been investigated and developed, by using zirconia- or ceria-based electrolytes. Use of cheap ferritic stainless steel is preferred [1–11], as it allows to reduce drastically the amount of ceramic materials and the costs [12]. The metal substrate is traditionally employed at the fuel compartment because of the reducing environment. The MSCs have demonstrated high strength whose mechanical properties are largely inherited from the metal substrate. Nowadays, MS-SOCs are approaching the commercialization stage with prototypes in the power range of 100 kW up to 1 MW running in a fuel cell or an electrolysis mode [13, 14]. This is possible with ceria as an electrolyte owing to its good thermo-mechanical compatibility with ferritic stainless steels, and its moderate sintering temperature ∼1100 °C [15]. Moreover, the relative amphoteric character of ceria with a smith acid-base parameter $\alpha = -2.7$ [16] prevents excessive affinity with amphoteric compounds such as Cr oxides (e.g. $Cr_2O_3$) which can be volatile and are inherently formed in MS-SOC as an oxidation product from the stainless steel [17,

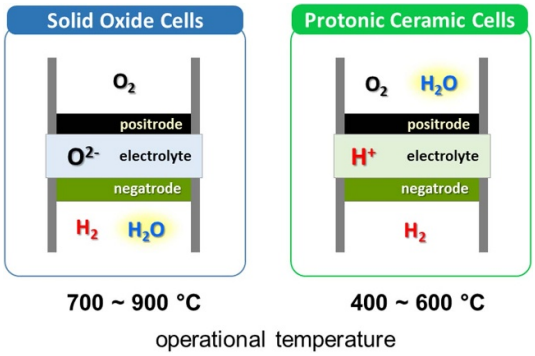


**Figure 1.** Difference of steam production/steam supply between SOC and PCC in fuel cell/steam electrolysis operation.

18]. In the case of electrolysis operation, however, the number of the operational studies with MS-SOC is yet limited [19–22] and there is in general very little information about long term durability which raises the question of the resistance of the metal substrate to the corrosion when exposed to a high steam concentration that is required for commercial applications. This issue may be mitigated when PCC is used as the electrolyte. As depicted in figure 1, geometric layout of PCC is different from SOC, in terms of steam production in fuel cells and steam supply in electrolysis cells. This ensures low oxygen partial pressure in the fuel electrode or negatrode compartment, and mitigates the risk of metal support corrosion in MSC architecture.

### 1.1. Proposed architectures for MS-PCC

In the electrochemical devices, the reaction takes place at the electrodes on each side of the electrolyte, therefore the functional electrodes have crucial roles that determine the performance. In the high temperature devices, the chemical reactants/products are in gaseous phase that are ionized at the electrodes. Thus, the electrodes must possess sufficient gas permeability to the electrolyte surface, good catalytic activities and a good electronic conductivity to achieve high electrochemical performances. On the other hand, the electrolyte should be gas tight, while the ohmic resistance is determined by the electrolyte thickness, i.e. the electrolyte layers need to be dense and as thin as possible. In the case of PCC, the State-of-the-Art electrolyte is made of perovskite oxides, of which refractory nature requires sintering at very high temperatures typically above 1400 °C, that makes it difficult to manufacture gas tight PCC electrolyte on the porous metal supports through the conventional ceramic processing. In 2005, Ito *et al* reported promising performance of thin film PCC on Pd membrane as the hydrogen gas permeable and electronic conducting support [23]. The pulsed laser deposition (PLD) technique was employed to coat $BaCe_{0.8}Y_{0.2}O_3$ (BCY) electrolyte, avoiding high temperature sintering process and achieving a gas tight PCC electrolyte layer as thin as 0.7 $\mu$m. The fuel cell power density reached 0.9 and 1.4 W $cm^{-2}$ at the operating temperatures of 400 °C and 600 °C, respectively. It demonstrated the high potential of PCC devices, in a new architecture and via an alternative process of the PCC electrolyte. However, Pd membrane utilization for PCC device would be limited due to high material cost. In this review, the focus is on the materials for MS-PCC that could be feasible for industrial applications. If the supporting metal has no $H_2$ permeability, the support needs to be porous for gas permeation.

It is preferable to fabricate the fuel electrode/negatrode layers on the metal support to prevent a high oxidizing atmosphere for the metal. Figure 2 illustrates the comparison of the architectures between ceramic supported cell and MSC for PCC. Note that the ceramic support is conventionally made of NiO-PCC perovskite cermet that also works as fuel electrode/negatrode. Because of the poor mechanical robustness of PCC negatrode, the thickness of the ceramic supported is usually over 600 $\mu$m, whereas the MSC relies on the robustness of the metal support, which thickness could be less than 500 $\mu$m. The use of cermet electrode material is only in the functional layer (thickness ~20 $\mu$m), which could reduce the amount of NiO and PCC perovskite oxide by more than 90% utilized in MSC in comparison to ceramic supported cell. Depending on the processing routes, which will be discussed in the following, the electrolyte thickness could be significantly reduced in MSCs that will benefit the mitigation of ohmic loss. Apart from the MSC structure shown in figure 2, symmetric design with two porous metal support is also proposed that would help to prevent warping or cracking arising from residual mismatch between the metal and ceramic sintering shrinkage [24].

### 1.2. Metal support materials and protection layers

The state-of-the-art PCC electrolyte materials have higher sintering temperature compared to those of SOC. Therefore, one of the challenges in the development of MS-PCC is to find a feasible process to manufacture

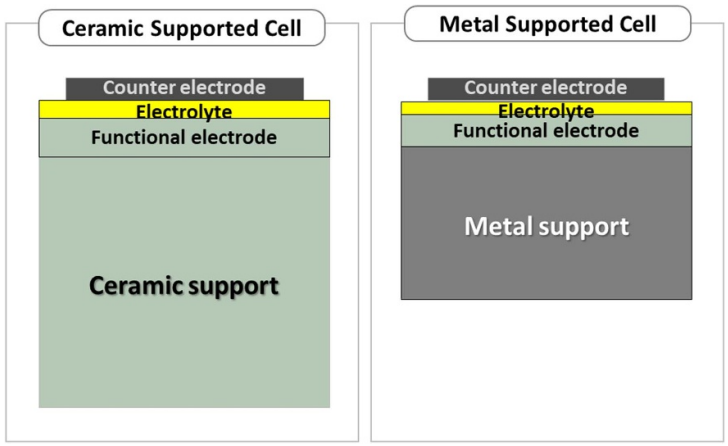


**Figure 2.** Schematic comparison of the architectures between ceramic supported and metal supported cells. Emphasis is on the difference in the cermet material consumption. The cermet utilization is only in the functional electrode layer in MSC, whereas it is dominated by the support in the ceramic supported cell.

gas-tight electrolyte on the porous metal without degrading the metal support and the electrolyte materials. Two processing routes are proposed for MS-PCC electrolyte layer. One is co-sintering process on shrinkable porous metal supports prepared by tape cast method using metal powder, for instance, and the other is deposition on non-shrinking substrates including the ceramic electrode layers on the porous metal, either sintered porous metals or metal plates with drilled pores. Considering material cost and oxidation resistance, ferritic steels are suitable for MSC. Metal support Materials for PCC reported in the literatures are summarized in table 1. They are all stainless steel with Cr content from 17% to 32%. Except for SUS316L containing 12% Ni, on which the applied layer had large cracks [25], metal support materials in the table 1 are ferritic steels (400-series stainless steels), of which thermal expansion coefficients (TECs) are reported between 10–12 $\times$ $10^{-6}$ $K^{-1}$ [25–27], comparable to those of conventional negatrode materials, i.e. cermet electrodes [28] and thus they are suitable for the support. Drawback of ferritic steel is Cr deposition/migration at high temperatures. When processed at high temperatures or operated at moderate temperatures in humidified condition, Cr deposition should be avoided to prevent degradation of the material and the performance by mitigating Cr evaporation from the metal and/or by eliminating Cr diffusion into functional layer in the cell processing and during the cell operation. Significant oxidation of metal support should also be avoided in MS-PCC process and in operation. Steam electrolysis with PCC does not need very high concentration of steam in the negatrode, however, it is well acknowledged that small amount of steam (2%–3%) in the PCC negatrode is needed for good performance and thus such an atmospheric condition with $H_2$ for a long-term operation could lead to the metal oxidation.

Venkatachalam *et al* tested four different tape casted alloys from Höganäs (Cr (20–32 wt.%) + Mn (0–0.4 wt.%)) for long term aging at 600 °C for 100 and 200 h in $H_2$/3%$H_2O$ after pre-oxidation at 800 °C for 2 h in $H_2$/3%$H_2O$ to form coherent scale [29]. Addition of 0.4 wt.% Mn in the metal would induce dual layer formation i.e. inner layer of chromia and outer layer of Mn–Cr spinel during high temperature treatment that work as the internal protective layer and minimizes further oxidation [29]. When the alloys were impregnated with rare earth elements such as Y, a protective external oxide could be formed by heat treatment, which showed significant reduction of weight gain during the oxidation. Oxidation of thin Co coating of commercial metal (Sanergy® HT, Sandvik, Sweden) was tested between 850 °C and 960 °C for 36 h in air [27]. Figure 3 shows the Co–Mn spinel formation on top of Cr oxide scale. Coated Co was identified as oxide spinel phase before annealing and was found to react with Mn contained in the ferritic steel to evolve the phase from $Mn_{0.3}Co_{2.7}O_4$ to $MnCo_2O_4$ from 850 °C to 960 °C. The SEM picture demonstrates that the Mn–Co spinel phase covers the Cr oxide layer to protect further evolution of Cr deposition. The drawback is that a high temperature annealing for a long time is required to form the spinel phase, which is not suitable for an industrial process.

The oxidation behavior of ferritic stainless-steel substrates with and without protective coating was investigated by Stange, Stefan *et al* [31, 33]. A metallic raw powder with 20.6 wt.% Cr and low Si content (<0.08 wt.%) (Höganäs AB, Sweden) was used to prepare porous metal support by aqueous tape casting yielding a relative density of 30%–35% after sintering at 1150 °C/2 h in 4% $H_2$/Ar. A protection layer of $La(Mn,Co)_{0.8}O_3$ was coated by infiltration of La, Co and Mn nitrate solutions under vacuum and fast curing at 900 °C, 30 s in air. The comparison of SEM pictures before and after applying the protective coating in

**Table 1.** Composition of the metals reported for MS-PCC applications. All metals are stainless steel, and minor elements are not indicated in the table. Material ratio is in wt%.

| | | Support fabrication | | |
|---|---|---|---|---|
| Material | Cr (%) | Process | Temp. (°C) atmosphere | References |
| SUS316L<br>TEC: $18.5 \times 10^{-6}$ $K^{-1}$ | 17<br>(12% Ni, 2% Mo) | Powder press | 1050 °C in vacuum | [25] |
| SUS430<br>TEC: $11.9 \times 10^{-6}$ $K^{-1}$ | 17 | Powder press | 1050 °C in vacuum | [25] |
| Ferritic steel alloys<br>(Höganäs AB, Sweden) | 20–32<br>(0–0.4%Mn) | Tape cast by Höganäs AB | 1250 °C in $H_2$ | [29] |
| Ferritic steel powders<br>(Sandvik, Sweden) | NA | Tape cast | 1100 °C–1300 °C 2 h in 4% $H_2$/Ar | [30] |
| Ferritic stainless steel<br>(Höganäs AB, Sweden) | 20.6<br>(Si $<$ 0.08%) | Tape cast<br>+ protective coating of $La(Mn_{0.5}Co_{0.5})_{0.8}$ by infiltration | 1100 °C–1300 °C in 4% $H_2$/Ar | [31–33] |
| Ferritic steel | 30 | Tape cast<br>CGO10 barrier layer<br>+ bridging layer | 1050 °C in 2% $H_2$/Ar | [34] |
| P434L, Ferritic steel | 17<br>(0.20% Mn) | Tape cast | 1050 °C in 2% $H_2$/Ar | [24, 34, 35] |
| ITM, Ferritic steel<br>(Plansee GmbH, Austria)<br>TEC: $11.3 \times 10^{-6}$/K | 26 | Commercial porous metal support | | [27, 36–38] |
| Sanergy-HT, Ferritic steel<br>(Sandvik, Sweden)<br>TEC: $12 \times 10^{-6}$ $K^{-1}$ | 17.5–18.5 | Commercial metal + drilled pores<br>(∼150 $\mu$m interval, diameter ∼50 $\mu$m) | | [27] |
| ZMG232L, Ferritic steel<br>(Hitachi Metals, Japan) | 22 | Commercial metal + drilled pores<br>(1 mm interval, diameter 200 $\mu$m) | | [39] |

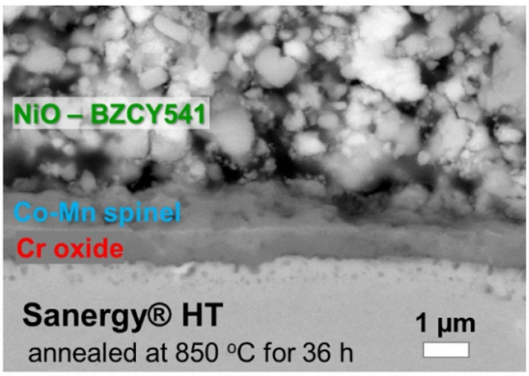


**Figure 3.** SEM cross section of the Sanergy® HT substrate coated with NiO-BZCY541 and annealed at 850 °C for 36 h in air. The phases determined by EDX mapping are indicated in the figure [27]. (BZCY541: $BaZr_{0.5}Ce_{0.4}Y_{0.1}O_{3-\delta}$) Reproduced from [27]. © 2021 ECS—The Electrochemical Society. All rights reserved.

figure 4 demonstrates that the coating wets the surface of the metal support. The thickness of the coating is inhomogeneous on the surface of the metal support and is found in excess in the trenches between the metal grains due to capillary effects. Specific mass gain of uncoated and coated samples in air and in

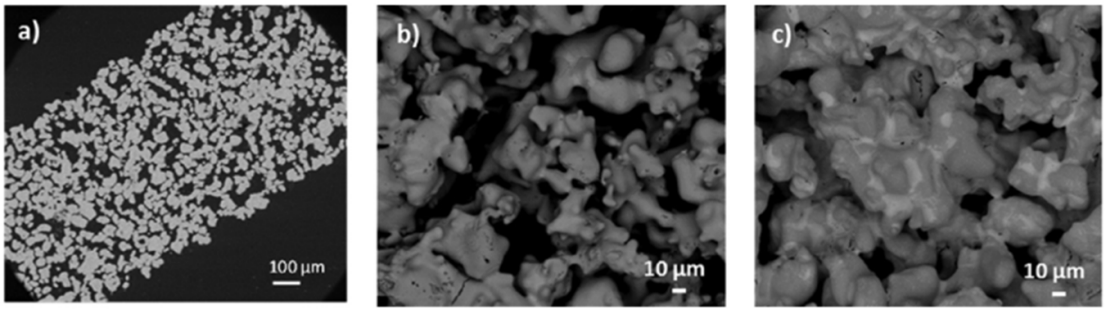


**Figure 4.** SEM micrographs of a metal support before and after $La(Mn_{0.5}Co_{0.5})_{0.8}$ protective coating; (a) cross section and (b) surface of a metal support after pre-annealing at 1175 °C, and (c) surface of a coated metal support after curing in air [31]. Reprinted from [31], Copyright (2017), with permission from Elsevier.

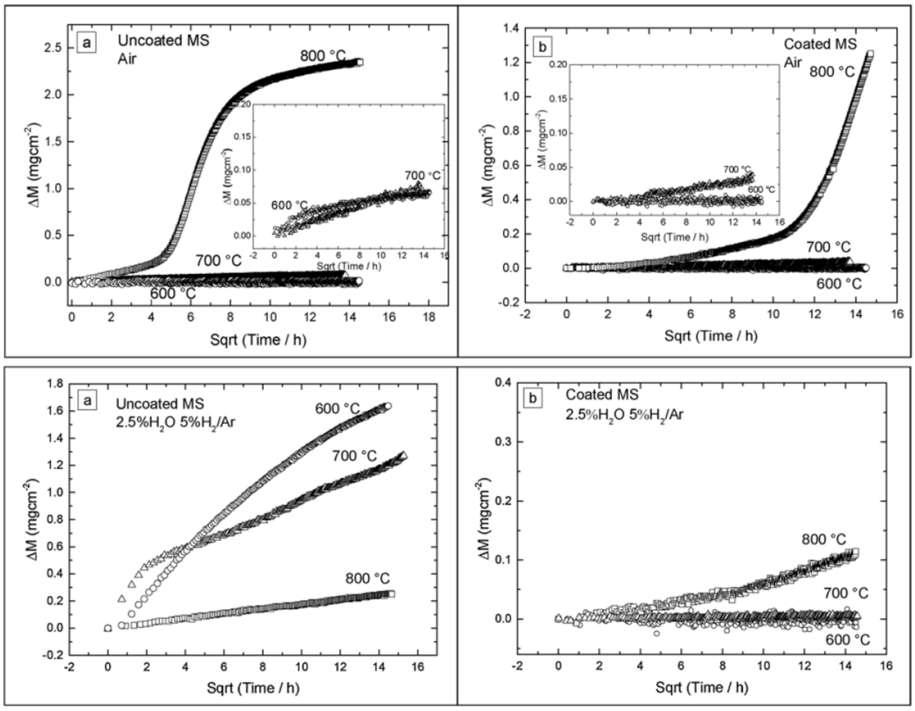


**Figure 5.** Specific mass gain as a function of the square root of time for porous metal support exposed at 600 °C, 700 °C or 800 °C in air (top) and in in $2.5\%H_2O/5\%H_2/Ar$ mixture (bottom) for ∼200 h: (a) uncoated metal supports; (b) coated metal supports [33]. Reprinted from [33], Copyright (2020), with permission from Elsevier.

$2.5\%H_2O/5\%H_2/Ar$ mixture are shown in figure 5, presenting isothermal oxidation at 600 °C, 700 °C and 800 °C. It demonstrates the oxidation kinetics in air changes drastically at 800 °C for both samples, while the profile of uncoated sample with an initial parabolic regime followed by break-away type kinetics indicates consumption of the entire metallic phase, whereas the initial protective regime is considerably longer for coated sample. In $2.5\%H_2O/5\%H_2/Ar$ mixture, the oxidation behavior of uncoated metal support was opposite to that in air. The lowest oxidation rate for the uncoated metal support was encountered at 800 °C that follows a single parabolic time dependence. The coated metal supports, on the other hand, demonstrate a more regular behavior. The results clearly demonstrate the beneficial effects of the coating on the oxidation rate, and particularly under reducing conditions. It was suggested outward diffusion of Cr is rate limiting the oxidation process when $Cr_2O_3$ forms as a protective oxide scale. Generally, chromia formers are prone to evaporation of chromium containing species at high temperatures, while the extent of evaporation is significantly reduced by the $La(Mn,Co)_{0.8}O_3$ protection coating.

It is reported Si and Cr migration occurs during co-sintering from the stainless steel to the PCC electrolyte, Y and/or Yb doped $Ba(Zr,Ce)O_{3-\delta}$, leading to formation of $Ba_2SiO_4$ and $BaCrO_4$ thus depletion of Ba from the proton conducting phase, while no significant migration of Ba, Zr, Ce, Y, or Yb into the metal upon co-sintering was observed [34]. The Ba loss in the $Ba(Zr,Ce)O_3$-based electrolyte is fatal for electrolyte

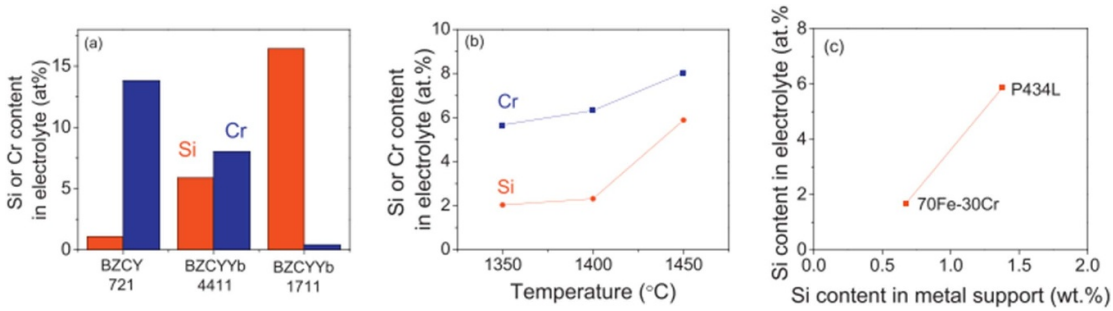


**Figure 6.** Si and Cr migration from the stainless-steel support to the electrolyte layer during co-sintering. Impact of (a) electrolyte composition, (b) sintering temperature, and (c) Si content in the metal support, as determined by EDS analysis. The support was P434L, the electrolyte was BZCYYb4411, and sintering temperature was 1450 °C, except as noted. Reprinted from [34], Copyright (2019), with permission from Elsevier.

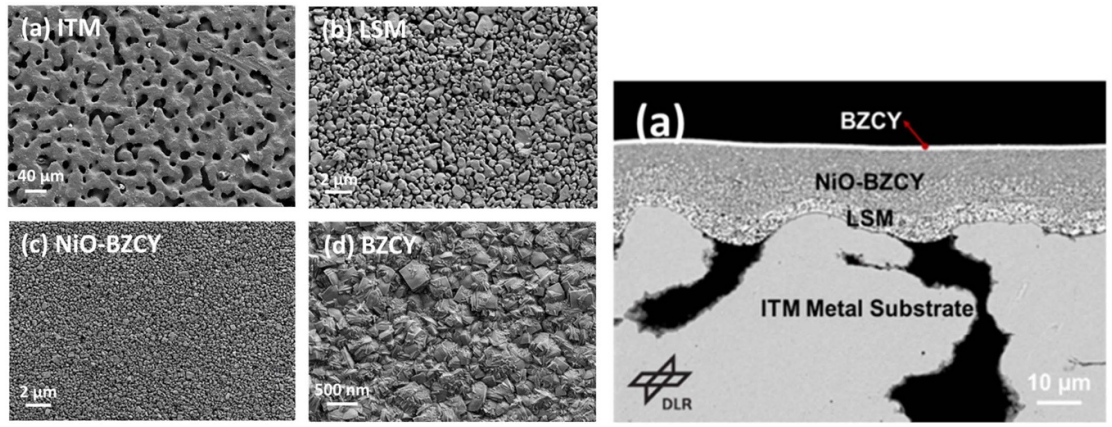


**Figure 7.** Scanning electron microscopy (SEM) image of the metal supported proton conducting cells. Surface micrographs of (a) ITM substrate, (b) LSM barrier layer, (c) NiO-BZCY541 negatrode, (d) PLD BZCY721 layer (left), and Cross-section SEM images of the MS-PCC cell at different magnifications (right). Reproduced from [38]. © 2021 ECS—The Electrochemical Society. All rights reserved.

performance due to low proton conductivity. Moreover, $Ba_2SiO_4$ and $BaCrO_4$ are inactive and would block the proton transport pathway. The extent of migration was determined for $BaZr_{0.7}Ce_{0.2}Y_{0.1}O_{3-\delta}$ (BZCY721), $BaZr_{0.4}Ce_{0.4}Y_{0.1}Yb_{0.1}O_{3-\delta}$ (BZCYYb4411), $BaZr_{0.1}Ce_{0.7}Y_{0.1}Yb_{0.1}O_{3-\delta}$ (BZCYYb1711) and for two ferritic steels with BZCYYb4411, and for three co-sintering temperatures (figure 6). Cr migration can be curtailed by lowering the sintering temperature below 1450 °C (figure 6(b)), since Si vapor pressure, Cr diffusivity, and reactivity between Si/Cr and BZCYYb4411 are reduced at lower temperatures. It is expected that Si evaporates from the metal and migrates via vapor diffusion, presumably creating a Si saturated atmosphere throughout the vicinity of the cell. In contrast, Cr is expected to migrate via solid state diffusion, consistent with the linear gradient in Cr concentration from the metal support to the exposed side of the electrolyte.

To avoid contamination from the metal support, other types of materials and manufacturing techniques of the protection layers or diffusion barrier layers (DBLs) on the metal support were investigated. Brandner *et al* reported $CeO_2$ DBL effectively prevented interdiffusion of cations between ferritic steel substrate and Ni-cermet anode [40]. $CeO_2$ or 10%–20% Gd-doped $CeO_2$ (CGO) were tested for MS-PCC support to reduce the Cr deposition in the ceramic layers [5, 30, 34]. PLD coated CGO was used as buffer layer between NiO-CGO electrode and very thin (<1 $\mu$m) $BaZr_{0.8}Yb_{0.2}O_{3-\delta}$ (BZYb20) electrolyte fabricated by PLD [39]. $CeO_2$ and CGO are well studied for different coating techniques, therefore they are good candidates for DBL and buffer layers. Perovskite oxides, $(La_{0.80}Sr_{0.20})_{0.95}MnO_{3-\delta}$ (LSM) was also tested to reduce the Cr diffusion towards Ni-cermet electrode layer [27, 37, 38]. LSM works also as an electrode and could be used for pore-downsizing layer. LSM layer application successfully reduce the pore size from 30 $\mu$m of the metal support down to a several hundred nm, which allows to fabricate functional electrode layer of finer microstructure and achieve a gas tight electrolyte coating by PLD (figure 7) [38].

It is one of the most critical issues for MS architecture to avoid metal oxidation and contamination from the metal that degrades the materials and therefore degrades their performance and limits their lifetimes. The porous structure of the metal support makes it more challenging to fabricate barrier layers on the metal

support. It is difficult to judge the effectiveness of each protection method due to limited number of researches demonstrated in operational conditions. It is therefore important to develop working cells and test their performance for long term to pursue suitable protection methods for MS-PCC.

### 1.3. Materials for the electrode layer and their manufacturing on the porous metal support

For fuel electrodes/negatrodes, which is usually fabricated on the metal support side, Ni-cermet with PCC electrolyte is typically used. The screen-print technique is commonly used to fabricate the porous electrode on the metal support. Exception is lamination of tape casted cermet layer [37, 38] and PLD [31, 32]. Lamination technique is relatively easier to fabricate smooth layer on macro porous surface; however, it is not easy to scale up. PLD was used to coat very thin $BaZr_{0.85}Y_{0.15}O_{3-\delta}$ (BZY15)-NiO film on top of spray coated $La_{0.5}Sr_{0.5}Ti_{0.75}Ni_{0.25}O_3$ (LSTN) layer [31, 36]. LSTN was used as intermediary layers between metal support and other thin film cell components implemented by PLD, and to utilize the exsolution of metallic Ni nanoparticles during operation for drop in the water splitting onset potential. Mercadelli *et al* investigated metal support material for PCC cermet anodes, NiO-BCZY ($BaCe_{0.65}Zr_{0.2}Y_{0.15}O_{3-\delta}$) [30]. The tape casted stainless-steel support was pre-sintered at 1100 °C–1300 °C for 2 h in 4% $H_2$/Ar and the DBL of $CeO_2$ and the NiO-BCZY layers were screen printed. They reported that the most critical issues for successful production of planar crack-free anode were found to be: (i) pre-sintering treatment of the metal support (1200 °C 2 h), (ii) presence of the DBL, (iii) thickness of the screen-printed films [30].

For the counter electrode, typically air side in this case, reported materials for MS-PCC electrochemical tests are $La_{0.6}Sr_{0.4}Co_{0.2}Fe_{0.8}O_3$ (LSCF) and Pt. LSCF is a very good electrode for SOC, and it has been reported to be operational as PCC electrode. More suitable and promising air electrodes for PCC are needed to be tested on MS-PCCs. From the recent progress of the following work of DLR group [38], $Ba_{0.5}Gd_{0.8}La_{0.7}Co_2O_{6-\delta}$ (BGLC)-BZCY541 composite electrode demonstrated promising performance on MS-PCC [41].

### 1.4. Electrolyte material—compatibility with metal support and stability in process conditions

For the PCC electrochemical devices, detrimental properties of electrolyte for high performance and long-term stability are high proton conductivity, low electronic current leakage, gas tightness, chemical stability, mechanical robustness under operational conditions. The state-of-the-art PCC electrolyte is Ba(Zr,Ce)$O_3$-based perovskite, which has chemical stability and high proton conductivity depending on the composition. Trivalent cations Y and Yb are the typical dopants in the perovskite, that are vital to raise the protonic conduction by increasing the hydration/proton incorporation into the perovskite lattice. The ratio between Zr and Ce determines the proton conductivity, the operational temperature range, the electronic current leakage, the chemical/mechanical stabilities, the TEC as well as the sinterability of the electrolyte. Electrolyte materials, process techniques and supporting layers investigated for MS-PCC are summarized in table 2.

The TECs of the state-of-the-art PCC, Y-doped $BaZrO_{3-\delta}$ (BZY) and Y-doped Ba(Zr,Ce)$O_{3-\delta}$ (BZCY) are $8 \times 10^{-6}$ and 9–10 $\times$ $10^{-6}$ $K^{-1}$, respectively [42, 43], which is smaller than those of the Ni-cermet and ferritic stainless steel. Stange *et al* investigated electrolyte deposition of modified composition of Sr- and Ce-doped proton-conducting electrolyte, $Ba_{0.85}Sr_{0.15}Zr_{0.7}Ce_{0.1}Y_{0.2}O_{3-\delta}$ (BSZCY151020), with higher TEC ($\sim$10–11 $\times$ $10^{-6}$ $K^{-1}$) [44] compared to BZY15, which reduced the risk of cracking of the electrolyte. BZY15 and BSZCY151020 were coated by PLD on top of the spray coated LSTN layer (TEC: $\sim$10–11 $\times$ $10^{-6}$ $K^{-1}$) on ITM (TEC: 11.3 $\times$ $10^{-6}$ $K^{-1}$) substrate at 600 °C. Post annealing at 650 °C in air of a sample with BZY15 electrolyte yielded significant cracking, while similar treatment of a sample with BSZCY151020 electrolyte resulted in no visible cracking [36].

As observed in figure 8, high temperature sintering process in reducing atmospheres used in co-sintering with the electrolyte layer may cause Ba loss in the Ba-based perovskite [34], which is fatal to degrade the proton conductivities [45, 46]. Viability of representative PCC electrolyte materials in the co-sintering process on the metal support were investigated [35]. The candidates were selected considering; (a) reported sintering temperature in the range 1200 °C–1600 °C to be close to the sintering temperature range for ferritic stainless steel of 1250 °C–1500 °C, and (b) conductivity of approximately $10^{-3}$ S $cm^{-1}$ or higher at 700 °C (figure 9) to enable reasonable resistance for an electrolyte layer of at least several microns thickness that can be produced by low-cost methods such as screen-print or tape-cast. The selected PCC electrolytes in different crystalline structures are pyrochlore ($La_{1.95}Ca_{0.05}Zr_2O_7$ (LCZ), $La_2Ce_2O_7$ (LCO)), perovskite ($Ba_3Ca_{1.18}Nb_{1.82}O_9$ (BCN), BZCY721), ($SrZr_{0.5}Ce_{0.4}Y_{0.1}O_3$ (SZCY541)) and acceptor doped rare-earth ortho-niobate ($La_{0.99}Ca_{0.01}NbO_4$ (LCN)). The coatings on P434L ferritic steel substrates were investigated by reducing atmosphere sintering, chemical compatibility with metal support during co-sintering, sintering behavior and evaporation during sintering. Among above representative PCCs, LCN was identified to be the most compatible for co-sintering with the metal support, as it can be densified at relatively low temperature

**Table 2.** PCC electrolyte materials and process techniques investigated for MS-PCC.

| Electrolyte layer | | | | | |
|---|---|---|---|---|---|
| Material | Process | Temp. (°C) | Thickness ($\mu$m) | Supporting layer | References |
| BZCYYb4411 + LiF | Sinter | 1350 | | Symmetric design with two metal supports | [24] |
| BZCYYb4411 + LiF | Sinter | 1350–1475 | | BZCYYb4411 + CGO10 barrier-bridging layer | [34] |
| BZCY721<br>SZCY541<br>BCN<br>LCZ<br>LCO<br>LCN | Sinter | 1450, 2 h<br>2% $H_2$–Ar | ∼10 | Infiltrated Sm-doped $CeO_2$ mixed with 20 vol.% Ni (SDCN catalyst) on tape casted P434L | [35] |
| SZY20 | PLD | 400 | 1.2 | Pd plating and SZY20 + LSCF by PLD (650 °C) | [25] |
| BZY15 | PLD | 600–700 | 3 | Protective coating of $La(Mn_{0.5}Co_{0.5})_{0.8}$ by infiltration (900 °C in air, 30 s)<br>Spray coated-$La_{0.5}Sr_{0.5}Ti_{0.75}Ni_{0.25}O_3$ (LSTN) | [31] |
| BSZCY151020 | PLD | 650 | 2 | Spray coated LSTN (600 °C–800 °C) | [36] |
| BZCY721<br>BSZCY151020<br>BZY15 | PLD | 650–700 | 1.5 | Laminated LSM + NiO-BZCY | [37] |
| BZCY721 | PLD | 700 | 1 | Laminated LSM + NiO-BZCY | [27, 38] |
| BZYb20 | PLD | 700 | <1 | +screen printed NiO-CGO10 anode (after filling the pores with NiO-CGO10) +CGO10/BZYb20/CGO10 electrolyte by PLD<br>CGO10 = buffer layer | [39] |
| BZCY721 BZY10 | EB-PVD | 725 | 1–1.5 | Dip coated LSM + screen printed NiO-BZCY | [27] |

(1300 °C), it does not evaporate component elements during sintering, and most importantly it does not react with the metal support (table 3). However, the cell ohmic impedances of LCN is too high for practical fuel cell or electrolysis cell application.

### 1.5. Co-sintering process for dense electrolyte layer

For industrial process, co-sintering is attractive technique due to the conventional low-cost, high-throughput manufacturing techniques for ceramic layer deposition (e.g. tape-cast, screen-print, aerosol spray deposition), which usually resulting in high density and good proton conductivity of the electrolyte layers due to high processing temperature, in comparison to physical vapor deposition (PVD) technique.

Sintering behavior of State-of-the-art PCC electrolyte, BZCY721, BZCYYb4411 and BZCYYb1711 were investigated and sinterability on P434L-ferritic steel supports with CGO10 bridging and CGO10 barrier layers were tested [34]. Sintering of the electrolyte pellets at 1450 °C for 2 h in 2% $H_2$/Ar atmosphere resulted in densification 73%, 94% and 98% for BZCY721, BZCYYb4411 and BZCYYb1711, respectively. Sintering aids were tested to find that LiF improves the density of BZCY721 to 94% in reducing atmosphere. With

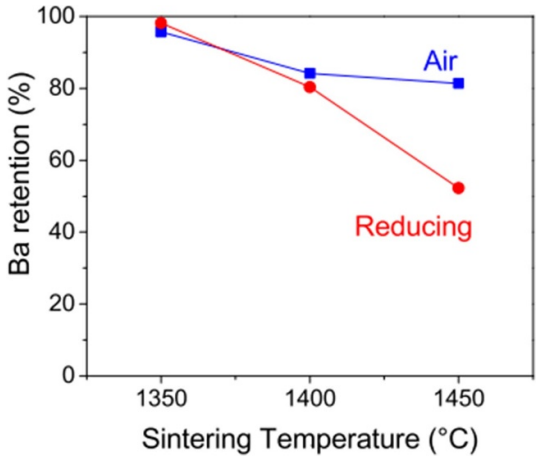


**Figure 8.** Impact of sintering temperature and sintering atmosphere on Ba loss. Ba content of ~10 $\mu$m BZCYYb4411 electrolyte film after sintering at various temperatures in air or reducing atmosphere, normalized to as-received powder. Reprinted from [34], Copyright (2019), with permission from Elsevier.

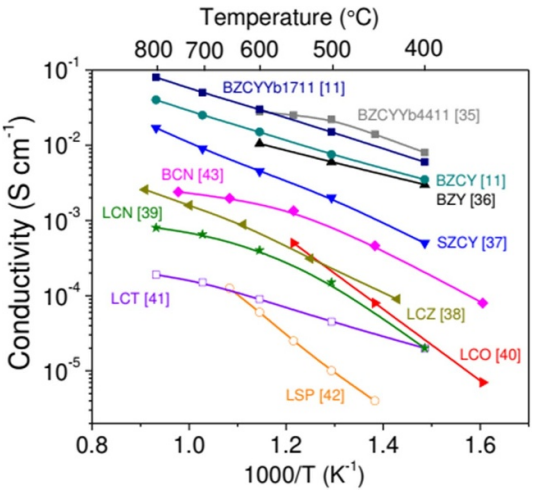


**Figure 9.** Conductivities of representative proton conductors. Reprinted from [35], Copyright (2019), with permission from Elsevier.

2 wt.%-LiF sintering aid, BZCYYb4411 sintering temperature could be reduced down to 1300 °C with the porous cermet on the metal support by co-sintering process [34]. Lower sintering temperature is beneficial for minimizing Si and Cr migration, preventing over-densification of the metal support, reducing Ba evaporation, and reducing processing cost.

The symmetric cell architecture developed and investigated at LBNL includes thin ceramic electrolyte and scaffold backbone layers co-sintered between ferritic steel supports. The architecture is attractive that could prevent warping or cracking due to residual mis-match between the materials [24]. Another benefit of the symmetric structure is that the electrolyte layer is not directly exposed to the flowing reducing atmosphere in the sintering furnace. The final Ba content in the sintered electrolyte was found to be nominally the same as in the starting powder. In contrast, the portion of the electrode near the highly porous metal support loses a significant amount of Ba. For the co-sintering process, improved shrinkage matching between BZCYYb and metal support is needed to minimize stress in the ceramic layer [24].

### 1.6. PVD for dense electrolyte coating

As summarized in the table 2, many of the work utilized PLD for electrolyte coating. PLD is an advanced technic among various PVDs for thin film deposition suitable for complex materials such as doped perovskite oxides. The PLD process can transfer the chemical composition as in the target and the deposited layer has a good crystallinity. However, due to the high running cost, limited deposition area and slow deposition rates, PLD technique is not suitable for large manufacturing process and remains limited to fundamental research.

**Table 3.** Summary of screening results for proton conductors suitable for co-sintering fabrication of metal supported cells [35]. Reprinted from [35], Copyright (2019), with permission from Elsevier.

| Family | Candidate | Representative composition | Survives sintering in reducing atmosphere? | Survives re-oxidation? | React with metal? | Densifies at 1450 °C or lower? | Evaporation during sintering? |
|---|---|---|---|---|---|---|---|
| Pyrochlore | LCZ | $La_{1.95}Ca_{0.05}Zr_2O_7$ | No | No | — | — | — |
| | LCO | $La_2Ce_2O_7$ | No | Yes | Yes–Cr, Si | — | — |
| Perovskite | BCN | $Ba_3Ca_{1.18}Nb_{1.82}O_9$ | Yes | Yes | Yes–Cr, Si | Falls apart | Yes |
| | BZCY | $BaZr_{0.7}Ce_{0.2}Y_{0.1}O_3$ | Yes | Yes | Yes–Cr, Si | Marginal | Yes |
| | SZCY | $SrZr_{0.5}Ce_{0.4}Y_{0.1}O_3$ | Yes | Yes | Yes–Si | Yes | Yes |
| Acceptor doped rare-earth ortho-niobate | LCN | $La_{0.99}Ca_{0.01}NbO_4$ | Yes | Yes | No | Yes | No |

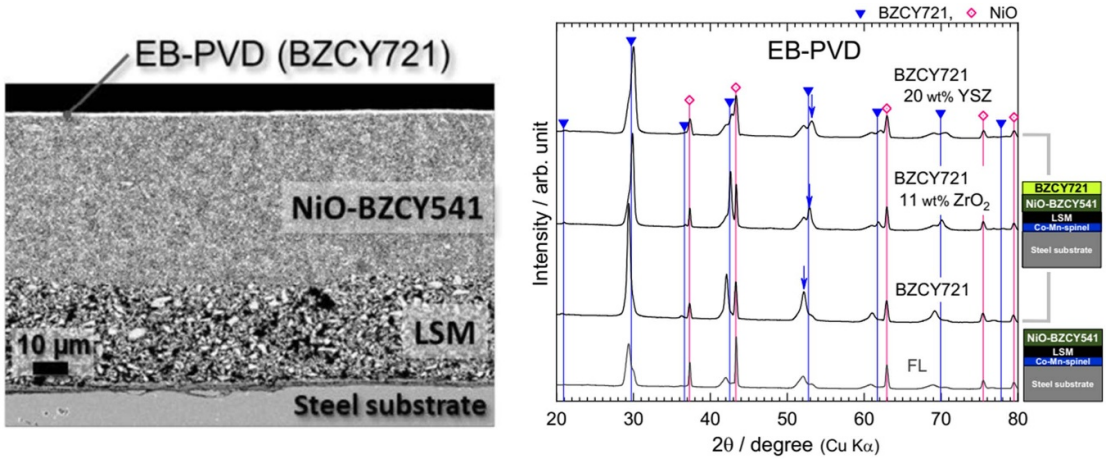


**Figure 10.** SEM cross section of the MS-PCC with 1 $\mu$m-thick BZCY721 electrolyte coated on porous ceramic layers of LSM and NiO-BZCY541 on the laser drilled metal support of Sanergy® HT at 725 °C by EB-PVD (left). LSM and NiO-BZCY541 were fabricated by dip coating and screen print method, respectively. XRD patterns of the half cells with thin film electrolyte by EB-PVD (right). The blue arrows indicate diffraction peaks of perovskite phase near 53°, demonstrating the peak shifts with added Zr source in the feed material [27]. Reproduced from [27]. © 2021 ECS—The Electrochemical Society. All rights reserved.

There are many other PVD techniques well developed and applied for many materials, and are usually less expensive than PLD. Most of the PVD can deposit on relatively large area and at higher deposition rate compared to PLD, while one of the drawbacks is difficulty in stoichiometric material transfer from the PVD source to the substrate, causing phase shift and inappropriate property in the coatings. Electron-beam PVD (EB-PVD) was tested for BZCY721 electrolyte coating process [27] (figure 10). When evaporation material of the targeting composition BZCY721 is used, XRD patterns of the coated layers show a BZCY perovskite phase but significant peak shifts were observed. Chemical composition analysis of the layer clarified the sputtering rates of the light elements Zr and Y were remarkably lower than those of the heavy elements Ba and Ce in the case of EB-PVD, which resulted remarkable compositional shift in the electrolyte layer. It was demonstrated that by controlling the elemental ratio in the feed source with additional Zr source, such as $ZrO_2$ powder, the chemical composition could be adjusted to achieve the targeted phase in EB-PVD and no secondary phase formation was observed. Further investigation of the thin film property was made by chemical composition assessment and impedance spectroscopy on EB-PVD coated BZCY721 thin films on sapphire substrates. It was clarified that thin films of reasonable proton conductivity were obtained when the composition was well adjusted [28]. The technique provides very homogeneous thickness (variation of less than $\pm$5%) with no composition gradient over the full deposition area allowing electrolyte coating on industrial cell size of $\sim$150 cm$^2$. Deposition rate is about 1 h for 1 $\mu$m thickness. Those features suggest that the EB-PVD technique would be suitable for industrial process.

Comparison of the manufacture techniques for the thin film electrolyte in MS-PCC is given in table 4. For its low cost and scalability, conventional sintering is a preferable option for manufacturing dense

**Table 4.** Comparison of potential thin film process techniques for MS-PCC electrolytes. Typical sintering/deposition temperatures and atmospheres plausible for MS-PCC are compared in this table. Suitability for industrial process is indicated by the symbols, in the order of ◯, △, and ×.

| Method | | Temp. °C | Atmosphere | Cost | Scalable | Advantages/*Issues* |
|---|---|---|---|---|---|---|
| Sintering | Co-sintering | 1300–1500 | Reducing ($H_2$, vacuum) | ◯ | ◯ | Conventional technique<br>*High residual stress*<br>*Ba loss* |
| | Constrained sintering | | Reducing ($H_2$, vacuum) | ◯ | ◯ | Conventional technique<br>*High residual stress*<br>*Densification of electrolyte*<br>*Ba loss* |
| PVD | PLD | <750 | $O_2 \lesssim$ Pa | × | × | Stoichiometric transfer<br>High crystallinity |
| | Electron beam PVD | | $O_2 < 1$ Pa | △ | ◯ | *Compositional shift* |
| | RF-sputtering | | Ar, $O_2 \sim$ Pa | △ | ◯ | *Compositional shift* |
| | Reactive magnetron sputtering | | Ar, $O_2 \sim$ Pa | △ | ◯ | High deposition rate<br>*Compositional adjustment for complex material* |

electrolyte layers, however, it is hard to avoid Ba loss of the BZCY electrolyte when sintering temperature is high and the atmosphere needs to be reducing condition that are required for electrolyte densification and preventing oxidation of the metal support. Moreover, it would be hard to reduce the electrolyte thickness less than several $\mu$m while achieving gas tightness in a large scale via sintering techniques. PVD grows electrolyte crystal layers by depositing the component atoms and molecules on the substrate, therefore the electrolyte thickness could be easily tuned in the range of 1 $\mu$m, which limit would be determined by the roughness of the porous electrode layers to achieve gas tight electrolytes. PLD is an ideal technique for such complex oxide materials like BZCY and has been used so far for MS-PCC, however, it is too expensive and limited yet to lab researches. Apart from the PLD, the main issue of PVD techniques is compositional adjustment. Due to the differences of component elements in the complex electrolyte, deposition rate of each element could differ that leads to a significant compositional shift in the deposited layer from that of the target and results in low proton conductivity of the electrolyte. A cost effective and scalable PVD technique should be developed for MS-PCC industrial process.

### 1.7. Electrochemical test

Electrochemical performance tests of the developed MS-PCCs were attempted, but very limited work succeeded to demonstrate the performance. Table 5 summarizes the OCV and area specific resistance (ASR) reported for MS-PCC. Most of the performances are still very low due to incomplete electrolyte gas tightness. Reasonable OCV over 1 V was reported [35, 36, 47], however, ASR was very high. In this table, maximum power densities in fuel cell mode were reported for only one MS-PCC using Pd anode plated on the porous metal support 1.2 and 2.2 mW $cm^{-2}$ at 400 °C and 450 °C, respectively, which is 2–3 orders of magnitude lower than typically reported performance levels for PCCs [25]. The electrical conductivity was 1–2 orders of magnitude lower than those reported for bulk samples, which is often reported for PLD coated PCC electrolytes. Nonetheless, the low performance may be due to the low OCV and high overpotentials. Reasonable ASR values were reported in the MS-PCC using BSZCY151020 or BZCY721 electrolyte coated by PLD on Ni-BZCY negatrodes [37, 38]. It was also suggested the smooth surface of the top electrode layer is one of the keys to grow good crystalline PCC electrolyte by PLD. The same group showed the promising performance with the same concept, with an OCV up to 0.9 V maximum and a current density of ~850 mA $cm^{-2}$ (1.3 V) at 600 °C in steam electrolysis operation, by applying double Ni-BZCY electrode layers with finer microstructure on top to allow a more gas tight PLD electrolyte coating and by utilizing a BGLC-BZCY541 composite air electrode [41]. Since the electrolyte was deposited by PLD at 700 °C,

**Table 5.** OCV and ASR reported for MS-PCC.

| Metal support | Electrodes fuel, air | Electrolyte Material/process/thickness ($\mu$m) | OCV (V) | ASR ($\Omega$ cm$^2$) | References |
|---|---|---|---|---|---|
| Tape casted ferritic steel | Sm doped $CeO_2$–Ni, Pt | LCN/sinter 1300 °C/10 | 1.02/700 °C | 50/600 °C | 35, 47 |
| Pd on SUS430 | Pd (plated), LSCF | SZY20/PLD 400 °C/1.2 | 0.67/450 °C | | 25 |
| Tape casted ferritic steel | BZY15-Ni (PLD), Pt | BZY15/PLD 600 °C/3 | | 40/600 °C | 31 |
| ITM | LSTN, Pt | BSZCY151020/PLD 600 °C/2 | 1.016/400 °C | | 36 |
| ITM | Ni-BZCY, Pt | BSZCY151020/PLD 700 °C/1.5 | | 2.4/600 °C | 37 |
| ITM | Ni-BZCY, Pt | BZCY721/PLD 700 °C/1 | 0.32/600 °C | 4.92/600 °C | 38 |
| ZMG232L | Ni-CGO10, LSCF | CGO10/BZYb20/CGO10/PLD 700 °C/<1 | 0.65/600 °C | | 39 |

conventional sintering process of the air electrode could not be applied, therefore the microstructure of the air electrode should further be optimized by engineering the process parameters.

By using PVD techniques, the electrolyte thickness could be very thin providing the roughness of the electrode surface is small enough. Thin electrolyte layer is beneficial to minimize ohmic losses and to reduce its risk of fracture due to mechanical stress. On the other hand, PCC electrolytes exhibit oxygen ion and p-type conductions in addition to proton, whose transport rates vary with material composition, temperature range and working atmosphere. P-type leakage through the electrolyte is critical to achieve high energy conversion efficiency for PCC applications. Nakamura *et al* studied the influence of the p-type conduction in PCC on the energy loss in electrochemical energy conversion applications [48]. By using the model in BZY20, energy efficiency was calculated with the internal current leakage in the electrolyte. It was demonstrated that the current leak loss was dominant over ohmic loss when the electrolyte thickness is below threshold. The p-type conduction increases with oxygen partial pressure, therefore PCC applications such as fuel cells and steam electrolysis cells are severely affected. An electron blocking layer is proposed to be inserted between the electrolyte and the air electrode to solve this problem. In the case of low oxygen partial pressure on both electrodes, such as in electrochemical hydrogen pump operation, this is not the case and high faradaic efficiency could be achieved.

## 2. Conclusions

Based on the knowledges and the technologies in MS-SOC development, achievement and progresses are observed in the MS-PCC development in the last decade. A few working cells have been reported and many issues are recognized. It was shown that protective coating/buffer layers on the metal support, either commercial or tape casted, are effective to avoid Cr and Si migration towards electrode layers, and could help to coat PCC electrolyte of improved quality. The electrode layer will also be a key for high performance and long-term operation, since the mechanical and chemical stabilities needs to be enhanced, and microstructure should be optimized. Identifying good air electrode materials is also important. MS-PCC is capable to reduce the electrolyte thickness, however, due to hole conduction in oxidizing atmosphere, electronic leakage would be more significant when the electrolyte thickness is very small, which leads to low faradaic efficiency in fuel cell and electrolysis operation, and thus electronic barrier layer on the air side should be considered.

The MSC architecture is ideal for PCC and their potential is attractive for wide range of electrochemical energy conversion devices. The MS-PCC is still a nascent technology. There are lot of challenges and problems in MS-PCC development, and several breakthroughs are expected to overcome technological issues.

## Data availability statement

No new data were created or analyzed in this study.

## ORCID iDs

Noriko Sata https://orcid.org/0000-0002-3103-2051
Rémi Costa https://orcid.org/0000-0002-3534-1935

## References

[1] Bance P, Brandon N P, Girvan B, Holbeche P, O'Dea S and Steele B C H 2004 Spinning-out a fuel cell company from a UK University—2 years of progress at Ceres power *J. Power Sources* **131** 86–90
[2] Brandon N P *et al* 2004 Development of metal supported solid oxide fuel cells for operation at 500–600 °C *J. Fuel Cell Sci. Technol.* **1** 61–65
[3] Oishi N and Yoo Y 2009 Fabrication of cerium oxide based SOFC having a porous stainless steel support *ECS Trans.* **25** 739–44
[4] Leah R T, Brandon N P and Aguiar P 2005 Modelling of cells, stacks and systems based around metal-supported planar IT-SOFC cells with CGO electrolytes operating at 500–600 °C *J. Power Sources* **145** 336–52
[5] Hui S (R), Yang D, Wang Z, Yick S, Decès-Petit C, Qu W, Tuck A, Maric R and Ghosh D 2007 Metal-supported solid oxide fuel cell operated at 400–600 °C *J. Power Sources* **167** 336–9
[6] Xie Y, Neagu R, Hsu C-S, Zhang X and Decès-Petit C 2008 Spray pyrolysis deposition of electrolyte and anode for metal-supported solid oxide fuel cell *J. Electrochem. Soc.* **155** B407–10
[7] Hui R, Berghaus J O, Decès-Petit C, Qu W, Yick S, Legoux J-G and Moreau C 2009 High performance metal-supported solid oxide fuel cells fabricated by thermal spray *J. Power Sources* **191** 371–6
[8] Haydn M *et al* 2014 Multi-layer thin-film electrolytes for metal supported solid oxide fuel cells *J. Power Sources* **256** 52–60
[9] Dayaghi A M, Kim K J, Kim S, Park J, Kim S J, Park B H and Choi G M 2016 Stainless steel-supported solid oxide fuel cell with $La_{0.2}Sr_{0.8}Ti_{0.9}Ni_{0.1}O_{3-\delta}$/yttria-stabilized zirconia composite anode *J. Power Sources* **324** 288–93
[10] Udomsilp D *et al* 2020 Metal-supported solid oxide fuel cells with exceptionally high power density for range extender systems *Cell Rep. Phys. Sci.* **1** 100072
[11] Pirou S *et al* 2022 Production of a monolithic fuel cell stack with high power density *Nat. Commun.* **13** 1263
[12] Tucker M C 2020 Progress in metal-supported solid oxide electrolysis cells: a review *Int. J. Hydrog. Energy* **45** 24203–18
[13] Leah R *et al* 2021 Commercialization of the Ceres power SteelCell® technology: latest update *ECS Trans.* **103** 679–84
[14] Ceres Homepage (available at: www.ceres.tech/) (Accessed 2023)
[15] Leah R T, Bone A, Selcuk A, Corcoran D, Lankin M, Dehaney-Steven Z, Selby M and Whalen P 2011 Development of highly robust, volume-manufacturable metal-supported SOFCs for operation below 600 °C *ECS Trans.* **35** 351–67
[16] Smith D W 1987 An acidity scale for binary oxides *J. Chem. Educ.* **64** 480–1
[17] Stenzel A, Fähsing D, Schütze M and Galetz M C 2019 Volatilization kinetics of chromium oxide, manganese oxide, and manganese chromium spinel at high temperatures in environments containing water vapor *Mater. Corros.* **70** 1426–38
[18] Huang W, Huang T, Song P, Chen R, Zheng B, Wang C, Li C and Lu J 2021 $CrO_2(OH)_2$ volatilization rate and oxidation behavior prediction of the NiCr coating in air-$H_2O$ environment at 650 °C *Corros. Sci.* **182** 109303
[19] Schiller G, Ansar A, Lang M and Patz O 2010 High temperature water electrolysis using metal supported solid oxide electrolyser cells (SOEC) *Adv. Sci. Technol.* **72** 135–43
[20] Nechache A, Han F, Semerad R, Schiller G and Costa R 2017 Evaluation of performance and degradation profiles of a metal supported solid oxide fuel cell under electrolysis operation *ECS Trans.* **78** 3039–47
[21] Welander M M, Hu B and Tucker M C 2023 Optimization of metal-supported solid oxide electrolysis cells with infiltrated catalysts *Int. J. Hydrog. Energy* **48** 21578–85
[22] Hagen A, Caldogno R, Capotondo F and Sun X 2022 Metal supported electrolysis cells *Energies* **15** 2045
[23] Ito N, Iijima M, Kimura K and Iguchi S 2005 New intermediate temperature fuel cell with ultra-thin proton conductor electrolyte *J. Power Sources* **152** 200–3
[24] Lau G Y and Tucker M C 2021 Development of metal-supported proton conducting solid oxide cells via co-sintering *ECS Trans.* **103** 685–92
[25] Kariya T *et al* 2016 Development of a novel cell structure for low-temperature SOFC using porous stainless steel support combined with hydrogen permeable Pd layer and thin film proton conductor *J. Alloys Compd.* **654** 171–5
[26] Tucker M C 2010 Progress in metal-supported solid oxide fuel cells: a review *J. Power Sources* **195** 4570–82
[27] Sata N, Han F, Zheng H, Dayaghi A M, Norby T, Stange M, Semerad R and Costa R 2021 Development of proton conducting ceramic cells in metal supported architecture *ECS Trans.* **103** 1779–89
[28] Sata N, Han F, Semerad R, Iguchi F, Ishii A, Takamura H, Riegraf M and Costa R, Perspectives and challenges for cost-effective manufacturing of robust protonic ceramic cells in metal-supported architecture *SSPC-21* (*Fukuoka, Japan, 17–22 September 2023*)
[29] Venkatachalam V *et al* 2014 Optimization of ferritic steel porous supports for protonic fuel cells working at 600 °C *Materials Science and Technology Conf. and Exhibition* vol 2 pp 1231–9
[30] Mercadelli E, Gondolini A, Pinasco P, Sanson A, Barison S and Fabrizio M 2011 Key issues in processing metal-supported proton conducting anodes for SOFCs applications *ECS Trans.* **35** 1761
[31] Stange M, Stefan E, Denonville C, Larring Y, Rørvik P M and Haugsrud R 2017 Development of novel metal-supported proton ceramic electrolyser cell with thin film BZY15-Ni electrode and BZY15 electrolyte *Int. J. Hydrog. Energy* **42** 13454–62
[32] Stefan E, Stange M, Denonville C, Larring Y, Hildenbrand N, Norby T and Haugsrud R 2017 Layered microstructures based on $BaZr_{0.85}Y_{0.15}O_{3-\delta}$ by pulsed laser deposition for metal-supported proton ceramic electrolyser cells *J. Mater. Sci.* **52** 6486–97
[33] Stefan E, Denonville C, Larring Y, Stange M and Hausgrud R 2020 Oxidation study of porous metal substrates for metal supported proton ceramic electrolyzer cells *Corros. Sci.* **164** 108335

[34] Wang R, Lau G Y, Ding D, Zhu T and Tucker M C 2019 Approaches for co-sintering metal-supported proton-conducting solid oxide cells with Ba(Zr,Ce,Y,Yb)$O_{3-\delta}$ electrolyte *Int. J. Hydrog. Energy* **44** 13768–76
[35] Wang R, Byrne C and Tucker M C 2019 Assessment of co-sintering as a fabrication approach for metal-supported proton conducting solid oxide cells *Solid State Ion.* **332** 25–33
[36] Stange M, Dayaghi A M, Denonville C, Larring Y, Rørvik P M, Haugsrud R and Norby T 2019 Fabrication of metal-supported proton-conducting electrolysers with thin film Sr- and Ce-doped BZY electrolyte *ECS Trans.* **91** 941–9
[37] Han F, Zhou X, Dayaghi A M, Norby T, Stange M, Sata N and Costa R 2019 Development of metal supported cells using $BaZrO_3$-based proton conducting ceramics *ECS Trans.* **91** 1035–45
[38] Zheng H, Han F, Sata N, Riegraf M, Dayaghi A M, Norby T and Costa R 2021 Metal supported proton conducting ceramic cell with thin film electrolyte for electrolysis application *ECS Trans.* **103** 693–700
[39] Miyamoto K, Kawabata T, Tachikawa Y, Matsuda J, Taniguchi S, Matsuzaki Y, Hayashi A and Sasaki K 2021 Preparation of model SOFCs with proton-conducting electrolytes on metal supports using pulsed laser deposition *ECS Trans.* **103** 2033–40
[40] Brandner M, Bram M, Froitzheim J, Buchkremer H P and Stöver D 2008 Electrically conductive diffusion barrier layers for metal-supported SOFC *Solid State Ion.* **179** 1501
[41] Costa R, Zheng H, Han F, Riegraf M and Sata N Progress in the development of metal-supported-cell architecture with proton conducting ceramics *EFCF 2022* (*Luzern, Switzerland, 5–8 July 2022*)
[42] Løken A, Ricote S and Wachowski S 2018 *Crystals* **8** 365
[43] Hudish G, Manerbino A, Coors W G and Ricote S 2018 Chemical expansion in $BaZr_{0.9-x}Ce_xY_{0.1}O_{3-\delta}$ (x = 0 and 0.2) upon hydration determined by high-temperature X-ray diffraction *J. Am. Ceram. Soc.* **101** 1298
[44] Dayaghi A M, Haugsrud R, Stange M, Larring Y, Strandbakke R and Norby T 2021 Increasing the thermal expansion of proton conducting Y-doped BaZrO3 by Sr and Ce substitution *Solid State Ion.* **359** 115534
[45] Yamazaki Y, Hernandez-Sanchez R and Haile S M 2010 Cation nonstoichiometry in yttrium-doped barium zirconate: phase behavior, microstructure, and proton conductivity *J. Mater. Chem.* **20** 8158–66
[46] Shima D and Haile S M 1997 The influence of cation non-stoichiometry on the properties of undoped and gadolinia doped barium cerate *Solid State Ion.* **97** 443–55
[47] Dogdibegovic E, Shen F, Wang R, Robinson I, Lau G Y and Tucker M C 2019 Progress in metal-supported solid oxide fuel cells and electrolyzers with symmetric metal supports and infiltrated electrodes *ECS Trans.* **91** 877–85
[48] Nakamura T, Mizunuma S, Kimura Y, Mikami Y, Yamauchi K, Kuroha T, Taniguchi N, Tsuji Y, Okuyama Y and Amezawa K 2018 Energy efficiency of ionic transport through proton conducting ceramic electrolytes for energy conversion applications *J. Mater. Chem.* A **6** 15771–80